Article

Current Biology

Iron and manganese availability drives primary production and carbon export in the Weddell Sea

Highlights

- The southern Weddell Sea had low primary production and carbon export
- FeMn input relieved FeMn co-limitation and changed species composition
- This led to higher primary production and highly carbon-rich aggregates

Authors

Jenna Balaguer, Florian Koch, Clara M. Flintrop, Christian Völkner, Morten H. Iversen, Scarlett Trimborn

Correspondence

jbalaguer@geomar.de

In brief

Balaguer et al. show that the southern Weddell Sea is FeMn co-limited as low Fe and Mn concentrations, primary production, and carbon export prevail. This study highlights that FeMn input can induce small but significant changes in plankton community composition and primary production, enhancing 4 times the carbon export potential.

Balaguer et al., 2023, Current Biology *33*, 4405–4414
October 23, 2023
https://doi.org/10.1016/j.cub.2023.08.086

CellPress

Current Biology

CellPress
OPEN ACCESS

Article

Iron and manganese availability drives primary production and carbon export in the Weddell Sea

Jenna Balaguer,[1,2,6,*] Florian Koch,[2] Clara M. Flintrop,[2,3,5] Christian Völkner,[2] Morten H. Iversen,[2,4] and Scarlett Trimborn[2]
[1]Marine Botany, University of Bremen, Bremen 28359, Germany
[2]Alfred Wegener Institute Helmholtz Centre for Polar and Marine Research, Bremerhaven 25570, Germany
[3]The Fredy & Nadine Herrmann Institute of Earth Sciences, Hebrew University of Jerusalem, Jerusalem 91904, Israel
[4]MARUM Center for Marine Environmental Sciences, University of Bremen, Bremen 28359, Germany
[5]Interuniversity Institute for Marine Sciences, Eilat 88103, Israel
[6]Lead contact
*Correspondence: jbalaguer@geomar.de
https://doi.org/10.1016/j.cub.2023.08.086

SUMMARY

Next to iron (Fe), recent phytoplankton-enrichment experiments identified manganese (Mn) to (co-)limit Southern Ocean phytoplankton biomass and species composition. Since taxonomic diversity affects aggregation time and sinking rate, the efficiency of the biological carbon pump is directly affected by community structure. However, the impact of FeMn co-limitation on Antarctic primary production, community composition, and the subsequent export of carbon to depth requires more investigation. *In situ* samplings of 6 stations in the understudied southern Weddell Sea revealed that surface Fe and Mn concentrations, primary production, and carbon export rates were all low, suggesting a FeMn co-limited phytoplankton community. An Fe and Mn addition experiment examined how changes in the species composition drive the aggregation capability of a natural phytoplankton community. Primary production rates were highest when Fe and Mn were added together, due to an increased abundance of the colonial prymnesiophyte *Phaeocystis antarctica*. Although the community remained diatom dominated, the increase in *Phaeocystis* abundance led to highly carbon-enriched aggregates and a 4-fold increase in the carbon export potential compared to the control, whereas it only doubled in the Fe treatment. Based on the outcome of the FeMn-enrichment experiment, this region may suffer from FeMn co-limitation. As the Weddell Sea represents one of the most productive Antarctic marginal ice zones, our findings highlight that in response to greater Fe and Mn supply, changes in plankton community composition and primary production can have a disproportionally larger effect on the carbon export potential.

INTRODUCTION

Phytoplankton fixes inorganic carbon into algal biomass via photosynthesis and thus provides organic carbon to the rest of the food web. This ultimately leads to export of carbon to deeper depth,[1] a process coined the biological carbon pump.[2] As a consequence, phytoplanktonic primary production in the Weddell Sea (south of 55°S–60°S)[3] accounts for ≈25% of the total Southern Ocean's (SO's) biological carbon uptake, making it one of the most productive marginal ice zones of the SO and an important area to study.[4] Large regions of the world's oceans, including the SO, display low phytoplankton biomass despite a plethora of available macronutrients. In the 1990s, John Martin and colleagues[5] discovered that iron (Fe) availability was the main factor for the lack of macronutrient utilization and the low chlorophyll biomass of these high nutrient low chlorophyll (HNLC) regions. The SO is the largest HNLC region where the scarcity of Fe and other trace metals (TMs), such as manganese (Mn), have previously been shown to impact phytoplankton growth.[6–11] This is not surprising since, in addition to low dissolved Fe (dFe) concentrations, low dissolved Mn (dMn) concentrations were also measured in several SO regions such as the Scotia Sea, Weddell Sea, and Drake Passage.[8,11–13]

It is well documented that phytoplankton cells have a high requirement for Fe, as it is required in many cellular metabolic pathways.[14,15] In addition to Fe, Mn is the second most needed TM involved in photosynthesis,[16] being an essential element of the metalloenzyme cluster of the oxygen-evolving complex during photosynthesis.[17] The fact that Mn may limit or, together with Fe, co-limit SO phytoplankton biomass, physiology, and productivity in the field has been demonstrated in several FeMn-enrichment experiments,[7,8,10,11] and their effects on carbon export have been projected in biogeochemical models.[18,19] Moreover, it has been shown that key members of the same phytoplankton community of the Drake Passage, such as the biogeochemically important diatom *Fragilariopsis*, were co-limited by Fe and Mn, whereas the other members were solely Fe limited.[11] In fact, different TM availabilities in seawater and the different TM requirements of different phytoplankton genera are key determinants of the plankton community composition.[14,20] The taxonomic composition of the phytoplankton community also influences how much carbon

is exported out of the mixed layer via the biological carbon pump, since taxonomic diversity of cell size and shape—for diatoms, different degrees of cell-wall silicification within a community—affect aggregation time and sinking rate.[21,22] For instance, a genus like the large and heavily silicified *Fragilariopsis* sp. acts as an important sinking conduit, as its thick silica frustules are less prone to dissolution and are more resistant to grazing than less silicified diatoms such as *Chaetoceros* sp.[22,23] Also, the colony-forming haptophyte *Phaeocystis antarctica*, which produces transparent exopolymer particles (TEPs), can form big aggregates[24] since TEP promotes the coagulation process and the formation of large particles.[25,26] In association with silicified diatoms, TEP-containing *Phaeocystis* aggregates can also sink,[27] potentially accelerating and facilitating carbon and silica export to the deep sea.[28] Thus, to model the primary production and subsequent carbon export by SO phytoplankton, it is crucial to understand the ecophysiology of key diatoms and *P. antarctica* in the SO. In this study, we investigated the potential of Fe and Mn to limit and/or co-limit primary production and impact phytoplankton composition at the genus level in the southern Weddell Sea. Furthermore, this is the first study that investigated the effects of TM limitation and co-limitation on aggregate formation, one of the main vectors for the transport of fixed organic carbon from the surface ocean to the deep sea, and quantified its potential for carbon export of a natural phytoplankton community of the Weddell Sea.

RESULTS AND DISCUSSION

Low Fe/Mn concentrations indicate FeMn co-limited phytoplankton across the southern Weddell Sea polynya

The seasonal polynya of the southeastern Weddell Sea is an understudied region (Figure 1A), primarily due to difficult access in the brief timeframe, where the area is not covered by ice. Hence, this study presents the first concentrations of dissolved TMs and their impacts on the phytoplankton community of this seasonally productive area. Surface concentrations of both total dFe and dMn were relatively low throughout the sampling region across our 6 stations (Table 1; Figure 1A) and coincided with low primary production rates (Table 1). In addition, *in situ* measurements of particulate organic carbon (POC) fluxes to 100 m depth measured from 3 sediment traps in the same study area (traps 1, 2, and 3; Table 1) were also low and consistent with previous values reported of Fe-limited waters,[29,30] indicating low carbon export fluxes. The additional calculation of an already published Mn deficiency coefficient in phytoplankton (Mn*, Table 1)[8] showed a relatively similar range of Mn* (−0.02 to 0.06 nmol L^{-1}) to previously reported Mn-limited and FeMn-co-limited phytoplankton populations of the Drake Passage (−0.02 to 0.04 nmol L^{-1}),[8] identified via FeMn amendment experiments. This further pinpointed that at the time when phytoplankton of the southern Weddell Sea were sampled, they were not primarily limited by Fe alone, but most likely FeMn co-limited. However, one must keep in mind that Mn* is highly dependent on the Fe and Mn requirements of each phytoplankton, which can greatly limit the use of the Mn* coefficient in the field. To test for FeMn co-limitation, an FeMn addition experiment was conducted with the *in situ* phytoplankton community sampled from location 1 (Figure 1A). The seawater used for the experiment was characterized by high macronutrient concentrations (nitrate + nitrite [NO_x] = 31.9 μmol L^{-1}; phosphate [PO_4] = 2.11 μmol L^{-1}; silicate [$SiOH_4$] = 69.5 μmol L^{-1}; Table 1) and low concentrations of dFe and dMn (0.16 and 0.08 nmol L^{-1}, respectively; Table 1). In line with this, the sampled phytoplankton community also exhibited a low photosynthetic efficiency (F_v/F_m, 0.26 ± 0.01; Table 2) and high functional absorption cross-sections of photosystem II (PSII) (σ_{PSII}, 9.69 ± 0.55; Table 2), both being representative of FeMn-limited waters.[31,32] In addition to the low dFe concentration (0.16 nmol L^{-1}, Table 1), which was indicative of Fe-limited HNLC waters (≈0.20 nmol L^{-1}),[33] the low dMn concentration (0.08 nmol L^{-1}, Table 1) was similar to values observed of FeMn-limited waters of the Drake Passage (≈0.03–0.4 nmol L^{-1}), to which FeMn additions were made,[7,8,11,34] and of the Mn-poor surface waters of the northern Weddell Sea (<0.2 nmol L^{-1}) based on which FeMn co-limitation was inferred.[35] Accordingly, at our sampling location, phytoplankton biomass was low, with concentrations of Chl*a*, POC, and primary production being 0.43 ± 0.02 μg L^{-1}, 0.22 ± 0.01 mg L^{-1}, and 17.0 ± 0.6 mg C m^{-3} day^{-1}, respectively (Table 1). The phytoplankton community was numerically dominated by a group of autotrophic pico-nanoflagellates (≈900 cells mL^{-1}; Table S1), already reported in SO Fe-poor waters.[36] Among the microplankton, diatoms were the dominant phytoplankton group, accounting for about ≈75% of the whole microphytoplankton community (Figure 1B). Among the diatoms, the heavily silicified *Fragilariopsis* sp., a genus commonly observed in SO HNLC waters,[11,37] was numerically the most abundant genus (75 cells mL^{-1}; Table S1). Another abundant genus was *Pseudo-nitzschia* sp. (54 cells mL^{-1}; Table S1), whereas *Chaetoceros* sp., *Corethron* sp., and *Leptocylindrus* sp. were only found with lower cell abundances (8, 5, and 18 cells mL^{-1}, respectively; Table S1). Consistent with observations made in other coastal regions of the SO, colonies of *P. antarctica* accounted numerically for 25% (52 cells mL^{-1}; Figure 1B; Table S1) of the total microphytoplankton community.[38,39] As in our study, diatoms and haptophytes (e.g., *P. antarctica*) represent important key players in the Weddell gyre.[40]

Chl*a*, POC-based growth rate and diatoms growth responded mostly to Fe

Although measurements of bulk community parameters such as Chl*a* are helpful, they may miss specific processes such as species-specific effects and TM co-limitation. Just as in our (Figure 2A) and numerous other studies,[8,11,41–43] Fe addition to the phytoplankton community of location 1 resulted in a total Chl*a* increase due to the high Fe requirement for Chl*a* synthesis.[14] Hence, Fe addition usually relieves chlorosis and enables the cells to increase their Chl*a* content.[44–46] Consistent with other studies,[8,11,41–43] POC and primary production of the whole community were strongly enhanced after the addition of Fe (Figures 2B and 2C). As 80% of the Fe requirement pertains to photosynthesis,[15,16] increased Fe supply, as an electron carrier, usually leads to more electrons being transported[47] and results in a greater rate of supply of ATP (adenosine triphosphate) and NADPH (nicotinamide adenine dinucleotide phosphate hydrogen) for carbon fixation. Based on our Chl*a* and POC results, the phytoplankton community as a whole was primarily limited by the availability of Fe. We also determined cell abundances of the most prominent microphytoplankton genera to

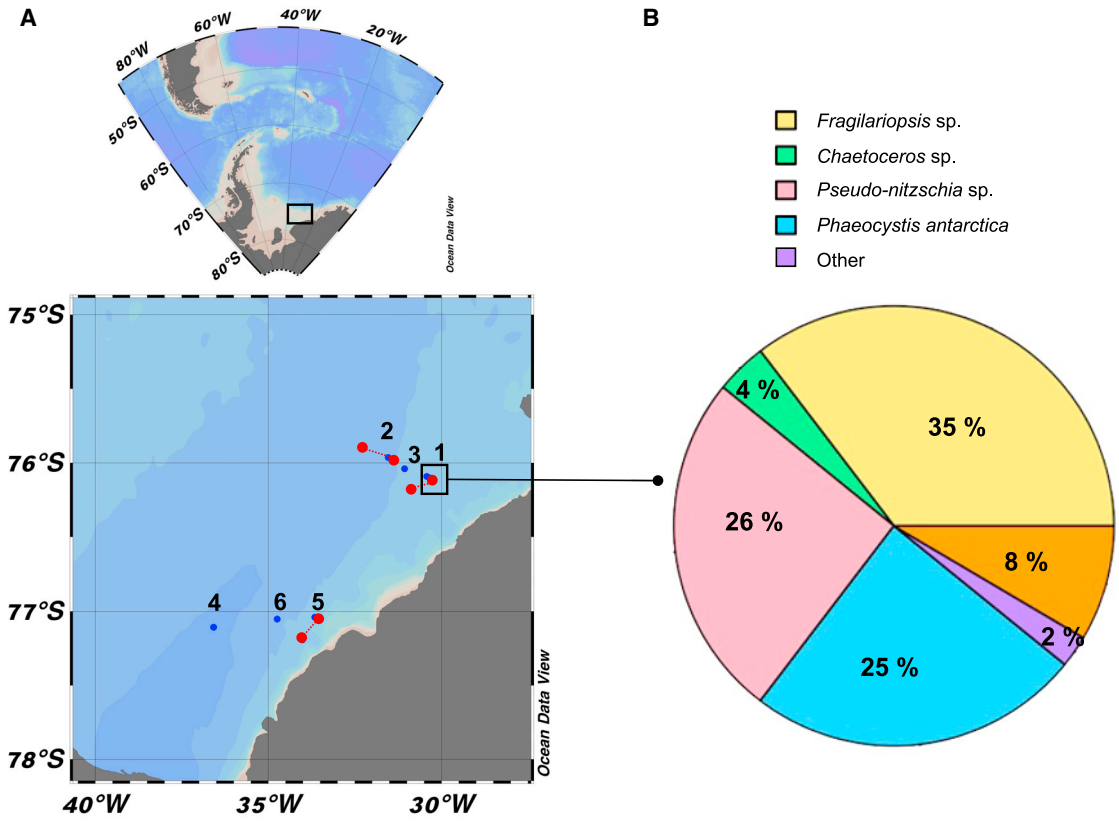

Figure 1. Overview of the sampling area in the Weddell Sea

Map showing (A) the 6 sampling locations and (B) the initial species composition of the experimental location. The blue points represent the stations as described in Table 1, and the connected red dots represent the deployment and the recovery of the drifting sediment traps as detailed in Table 1 (A). At location 1, an FeMn addition experiment was conducted with the *in situ* phytoplankton assemblage, which was initially composed of the shown different phytoplankton groups (B). Relative abundances of the main microphytoplankton genera (based on data from Table S1) at the start of the experiment were determined via light microscopy.

identify possible FeMn co-limitation effects at the genus level (Tables 3 and S1). Although the communities in all treatments remained numerically diatom dominated, the relative contribution of each genus changed depending on the different TM additions (Table. S1). After Fe addition, for instance, the growth rates of the two ecologically important diatoms *Fragilariopsis* sp. and *Chaetoceros* sp. significantly increased by ≈20% and ≈70%, respectively, relative to the control (Table 3). It has frequently been reported that these two diatom genera are the main beneficiaries of Fe-enrichment experiments in the field.[23,41,48] Interestingly, the addition of FeMn did not lead to any changes in the growth of these two genera relative to the Fe addition, suggesting that they were primarily Fe limited. In contrast, *Pseudo-nitzschia*'s ability to cope with a wide range of Fe concentrations[49] was also evident in this study by its lack of response to neither +Fe nor +FeMn (Table 3). Whether this was due to its low Fe requirement or to the limitation by another TM or vitamin is unclear. For example, SO phytoplankton species have previously been reported to be Fe and vitamin B_{12} co-limited[50,51] and/or to experience additional limitations by other TMs such as zinc and cobalt.[51] Nevertheless, it cannot be excluded that the overall great increase in growth of all species for each treatment (Table S1) may also be biased by possible bottle effects (e.g., lack of sinking and large grazers).[52,53]

FeMn co-limited *P. antarctica* drove increases in primary production

In line with Wu et al.,[10] in our study, the colonial *P. antarctica* was also FeMn co-limited, as it only achieved maximum growth when both TMs were provided (Table 3). In addition to this, significant species-specific TM effects inside the community were also observed. Although *P. antarctica* was FeMn co-limited, *Pseudo-nitzschia* sp. was not limited by the tested TMs, and *Fragilariopsis* sp. and *Chaetoceros* sp. were only Fe limited. Hence, this study highlights the complex effects of TM limitation and co-limitation at the genus level. Interestingly, in this study, responses to Fe and Mn availabilities differed even between bulk parameters. Although both Chl*a*-based growth rate and POC-based growth were driven by Fe alone, primary production reached its maximum only in the FeMn treatment, resulting in a +34% increase over Fe alone (157 ± 12 to 210 ± 34 mg C m^{-3} day^{-1}; Figure 2C). This increase in primary production was accompanied by a significantly higher growth rate of *P. antarctica* in the FeMn addition compared with the Fe addition (0.49 vs. 0.42 day^{-1}; Tables 3 and S1;). Additionally, not only the number of cells was increased but also more colonies were formed in the +FeMn treatment (Table S2). High Fe supply was previously found to trigger colony formation[54] but had never been tested in combination with Mn. Unlike single-celled

Table 1. Biological and chemical characterization of the experimental area (Figure 1)

	Latitude (° min^{-1})	Longitude (° min^{-1})	Surface total dFe (nmol L^{-1})	Surface total dMn (nmol L^{-1})	Mn* (nmol L^{-1})	NO_x (μmol L^{-1})	PO_4 (μmol L^{-1})	$SiOH_4$ (μmol L^{-1})	Chl*a* (μg L^{-1})	POC (mg L^{-1})	Primary production (mg C m^{-3} day^{-1})	Measured POC flux, POC_{100_insitu} (mg C m^{-2} day^{-1})
1 Experiment location	76°06.140	30°19.084	0.16	0.08 ± 0.01	0.02	31.9	2.11	69.5	0.43 ± 0.02	0.22 ± 0.01	17.0 ± 0.6	POC_{100_exp}, 92.2 ± 18.9 (calculated, see Table S3)
2	75°57.886	31°32.416	0.15 ± 0.03	0.04 ± 0.01	-0.02	–	–	–	–	–	13.6 ± 1.5	–
3	76°02.415	31°03.924	0.19 ± 0.03	0.13 ± 0.01	0.06	–	–	–	–	–	10.7 ± 0.6	–
4	77°06.455	36°34.869	0.37 ± 0.04	0.16 ± 0.01	0.02	–	–	–	–	–	41.8 ± 0.7	–
5	77°02.365	33°33.906	0.09 ± 0.01	0.09 ± 0.01	0.06	–	–	–	–	–	4.5 ± 0.3	–
6	77°03.018	34°44.548	0.18 ± 0.05	0.07 ± 0.07	0.00	–	–	–	–	–	8.6 ± 0.3	–
Sediment trap 1 deployment	75°58.599	31°22.128	–	–	–	–	–	–	–	–	–	–
Sediment trap 1 recovery	75°53.980	32°15.100	–	–	–	–	–	–	–	–	–	68.6
Sediment trap 2 deployment	76°05.541	30°25.299	–	–	–	–	–	–	–	–	–	–
Sediment trap 2 recovery	76°10.040	30°53.354	–	–	–	–	–	–	–	–	–	54.2
Sediment trap 3 deployment	77°02.405	33°39.240	–	–	–	–	–	–	–	–	–	–
Sediment trap 3 recovery	77°11.562	34°01.114	–	–	–	–	–	–	–	–	–	93.8

Concentrations of macronutrients (NO_x = NO_3 [nitrate] + NO_2 [nitrite]; PO_4, phosphate; $SiOH_4$, silicate), chlorophyll a (Chl*a*), and particulate organic carbon (POC) were determined in the seawater sampled at location 1 (Figure 1). Additionally, surface concentrations of total dFe, dMn, manganese deficiency (Mn*), and primary production were determined in the seawater sampled from 20 m depth at stations 1–6 (Figure 1). Particulate organic carbon flux to 100 m (POC_{100_insitu}) was determined from 3 sediment traps 1, 2, and 3 in the same area (Figure 1A) as well as at the end of the experiment (location 1). Values represent the mean ± SD (n > 3).

Table 2. Photophysiological response

	F_v/F_m (rel. unit)	σ_{PSII} (nm^2)
Initial	0.26 ± 0.01	9.69 ± 0.55
Control	0.28 ± 0.06c	9.82 ± 1.69a
+Mn	0.31 ± 0.04b	9.03 ± 1.47b
+Fe	0.31 ± 0.02b	7.89 ± 1.16c
+FeMn	0.36 ± 0.03a	7.52 ± 0.77c

The dark-adapted maximum photosystem II quantum yield (F_v/F_m) and the functional absorption cross-section of PSII (σ_{PSII}) were determined at the start and the end of the experiment from the communities after exposure to different Fe and Mn concentrations. Values represent the mean ± SD (n > 3). Different letters indicate significant differences at the 5% level from the higher mean (a) to the lowest mean (c).

Phaeocystis being more competitive for scarce Fe and Mn supply,[11,55] colonial *Phaeocystis* cells accumulate Fe and Mn in their mucus matrix[56] with the organic content of the mucus matrix supporting the photochemical reduction of Fe and Mn, thus increasing their bioavailability to *Phaeocystis*.[26,57,58] Hence, the accumulated dFe (0.5 nmol L^{-1}) and dMn (1 nmol L^{-1}) led to larger and more abundant *P. antarctica* colonies in the +FeMn treatments (Table S2). In an area like the SO, where the scarcity of Fe and Mn drives phytoplankton species composition, the ability of the colonial *Phaeocystis* to use its mucus as a TM reservoir may be a competitive advantage over other phytoplankton genera.[56]

P. antarctica enhanced the carbon export potential of the diatom-dominated plankton community

An aggregation experiment was conducted with the final phytoplankton communities of the four treatments to determine whether the observed changes in community composition also translate into a change in carbon export potential (see STAR Methods for detailed description). This is the first study that directly links the effects of FeMn additions on community composition changes and primary production together with aggregate formation and settling rates. From each treatment, resulting aggregates larger than 0.5 mm were picked and used for further analyses. The aggregate volumes were similar between the treatments, ranging from <0.1 to 8.2 cm^3, whereas the sinking velocities ranged from 0.5 and 40 m day^{-1} (Table S3). Very interestingly, the POC content of the aggregates changed with TM addition (POC_{end}, Table 4). Relative to the control, the POC content of the aggregate increased, although not significantly, in the +Mn treatment (+35%) and the +Fe treatment (+50%). The highest POC concentrations were observed in the FeMn-enriched aggregates (Table 4), likely due to the higher number of larger *P. antarctica* colonies formed upon FeMn addition (Table S2). Colonial *P. antarctica* cells have a mucilaginous matrix surrounded by a hydrophobic membrane; hence, when a colony is formed, organic matter, e.g., (muco)polysaccharides and carbohydrates, are exuded from the cell.[59] Approximately 30%–50% of the assimilated POC is located in the mucus matrix of a *P. antarctica* colony.[60,61] As the polysaccharide matrix of *Phaeocystis* colonies contains high amounts of TEP, it can facilitate aggregation due to its glue-like nature.[25,26] Our results show that the growth of colonial *P. antarctica* was significantly increased

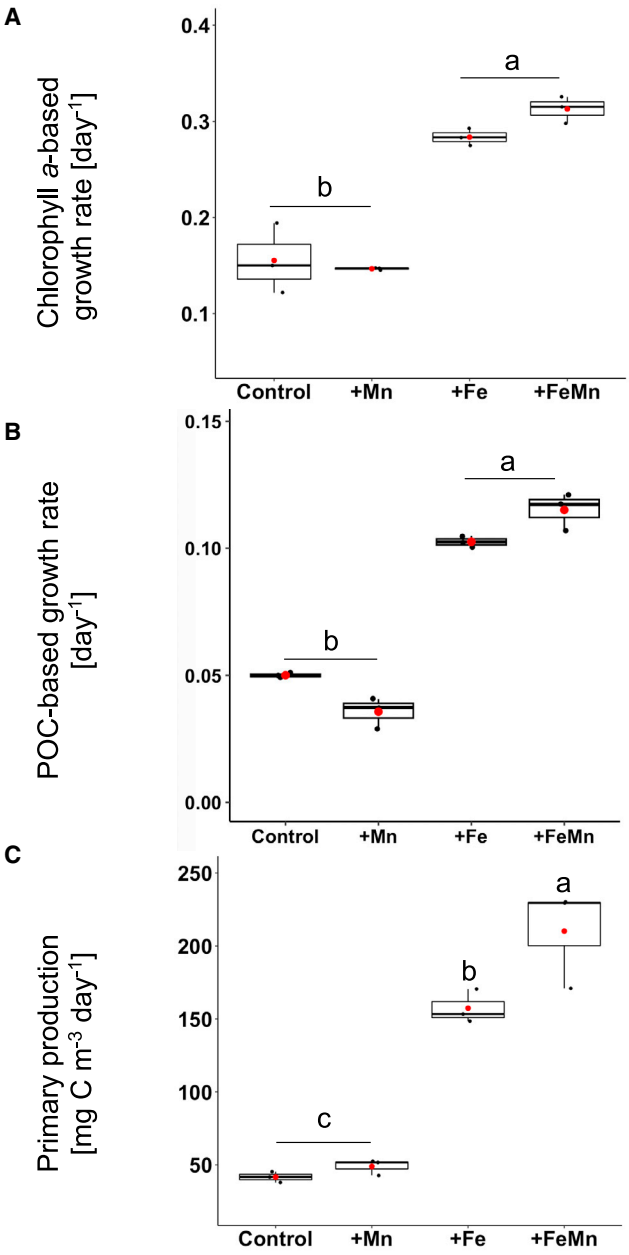

Figure 2. Community response

(A) Chlorophyll a-based accumulation rate, (B) particulate organic carbon production (POC) production, and (C) primary production were estimated from the communities after exposure to different Fe and Mn concentrations. Data are represented in box plots where the black points represent the individual replicates (n = 3), and the red points represent the mean (based on data from Table S5). Different letters indicate significant differences between treatments ($p < 0.05$).

when Fe and Mn were added together (+500%) over Fe alone (+210%), indicating FeMn co-limitation (Table S1). This change within the diatom-dominated phytoplankton community had, however, strong implications for primary production and its carbon export potential. Although Fe alone stimulated primary production by 270%, it only led to a 40% increase in potential

Table 3. Genus-specific response

	Fragilariopsis sp. (day^{-1})	*Chaetoceros* sp. (day^{-1})	*Pseudo-nitzschia* sp. (day^{-1})	*Phaeocystis antarctica* (day^{-1})
Control	0.46 ± 0.02b	0.34 ± 0.04b	0.45 ± 0.02a	0.22 ± 0.06^{c}
+Mn	0.46 ± 0.00b	0.33 ± 0.07b	0.38 ± 0.01b	0.21 ± 0.02^{c}
+Fe	0.56 ± 0.01a	0.57 ± 0.02a	0.45 ± 0.05a	0.42 ± 0.01b
+FeMn	0.57 ± 0.01a	0.58 ± 0.01a	0.49 ± 0.01a	0.49 ± 0.05a

Growth rates of *Fragilariopsis* sp., *Chaetoceros* sp., *Pseudo-nitzschia* sp., and *Phaeocystis antarctica* were determined via light microscopy after exposure to different Fe and Mn concentrations. Values represent the mean ± SD (n = 3). Different letters indicate significant differences at the 5% level from the higher mean (a) to the lowest mean (c).

carbon export to 100 m (POC_{100_exp}, Figure 3; Table 4). Relative to Fe alone, the combined addition of Fe and Mn only slightly enhanced primary production by +30%, but more interestingly, it enhanced the carbon export potential by +180%. Our study highlights that small changes in species composition and primary production can, however, have a disproportionally larger effect on the makeup of aggregates.

Ecological implications for the biogeochemistry of the southern Weddell Sea

Additional *in situ* measurements of POC fluxes to 100 m depth (POC_{100_insitu}; 72.2 mg C m^{-2} day^{-1} – average of traps 1, 2, and 3 in Table 1) fit the calculated carbon export for FeMn co-limited phytoplankton in the control treatment (POC_{100_exp}; station 1 in Table 1; Figure 3) at the end of the incubation experiment. These POC_{100_insitu} fluxes (station 1 and traps 1, 2, and 3; Table 1) were low and comparable with previous carbon export fluxes reported for Fe-limited waters.[29,30,62] For instance, at the Kerguelen Plateau,[30] carbon export fluxes of the naturally Fe-fertilized (≈276 mg C m^{-2} day^{-1}) *Phaeocystis* bloom were 2-fold higher relative to the unfertilized waters (≈146 mg C m^{-2} day^{-1}). Similarly, during the CROZet natural iron bloom and EXport experiment (CROZEX) campaign,[29] carbon export fluxes of the Fe-enriched patch (≈180 mg C m^{-2} day^{-1}) were 3 times higher relative to the fluxes of the unfertilized waters (≈60 mg C m^{-2} day^{-1}).[62] As sedimentary input of Fe is presumably accompanied by Mn as well,[63] both the surroundings of the Kerguelen and Crozet islands were most likely enriched in both Fe and Mn. In our experiment, in response to FeMn enrichment, POC_{100_exp} increased by 4-fold compared with the control (Figure 3; Table S3), henceforth, leading to reasonably similar fertilization effects as reported at the Kerguelen and Crozet islands.[29,30] Similar to our experimental station (location 1), concentrations of dFe and dMn, the Mn deficiency indicator as well as primary production and POC_{100_exp} (Table 1), were all low in the sampling area of the southern Weddell Sea (Figure 1A). Therefore, based on the results of our FeMn-enrichment experiment, we speculate that this region suffers from FeMn co-limitation and would likely respond to greater Fe and Mn supply with much higher carbon export fluxes.

For a long time, SO primary production has largely been deemed as being solely Fe limited since a plethora of Fe fertilization experiments resulted in enhanced primary production after Fe additions.[42] It needs to be noted that in addition to other factors such as aggregate fragmentation, grazing by zooplankton, and microbial remineralization,[58] the potential for carbon export is highly dependent on which functional type of phytoplankton acts as the carbon conduit.[22] The addition of different phytoplankton functional types into models is, therefore, crucial to assess the widespread effect of low Fe and Mn concentrations and the resulting effects on carbon production and export in the SO.[19] In most biogeochemical SO models, for example, *Phaeocystis* is not included as an additional functional group mostly due to its very complex life cycle,[39] although this study highlights that the increased growth of *P. antarctica* within a diatom-dominated phytoplankton assemblage significantly enhanced the potential carbon export. In line with our results, model simulations that incorporated characteristics of *P. antarctica* colonies revealed a possible overestimation of diatoms contributing to primary production and sinking of POC in the SO.[64] In fact, south of 60°S, in the Weddell or Ross Sea, models projected that *P. antarctica* colonies contribute up to 30%–50% of the total POC export.[64,65] Although we present results from a single experiment, it now becomes clear that low concentrations of both Fe and Mn prevail in many areas of the SO,[7,8,11,13,34,35,66] with diverse responses on phytoplankton functional types[11,19] and potentially, important implications for the biological carbon pump. Therefore, it is imperative that biogeochemical models integrate Mn limitation/FeMn co-limitation when considering future changes of TM input into SO surface waters, something which has only recently been implemented.[18,19]

STAR★METHODS

Detailed methods are provided in the online version of this paper and include the following:

- KEY RESOURCES TABLE
- RESOURCE AVAILABILITY
  - Lead contact
  - Materials and data availability
  - Data and code availability
- EXPERIMENTAL MODEL AND SUBJECT DETAILS
- METHOD DETAILS
  - Water collection for *in situ* sampling and one shipboard phytoplankton TM incubation experiment
  - TM seawater chemistry
  - Phytoplankton community characterization
  - Phytoplankton quotas
  - ^{14}C-based primary production
  - Photosystem II (PSII) fluorescence

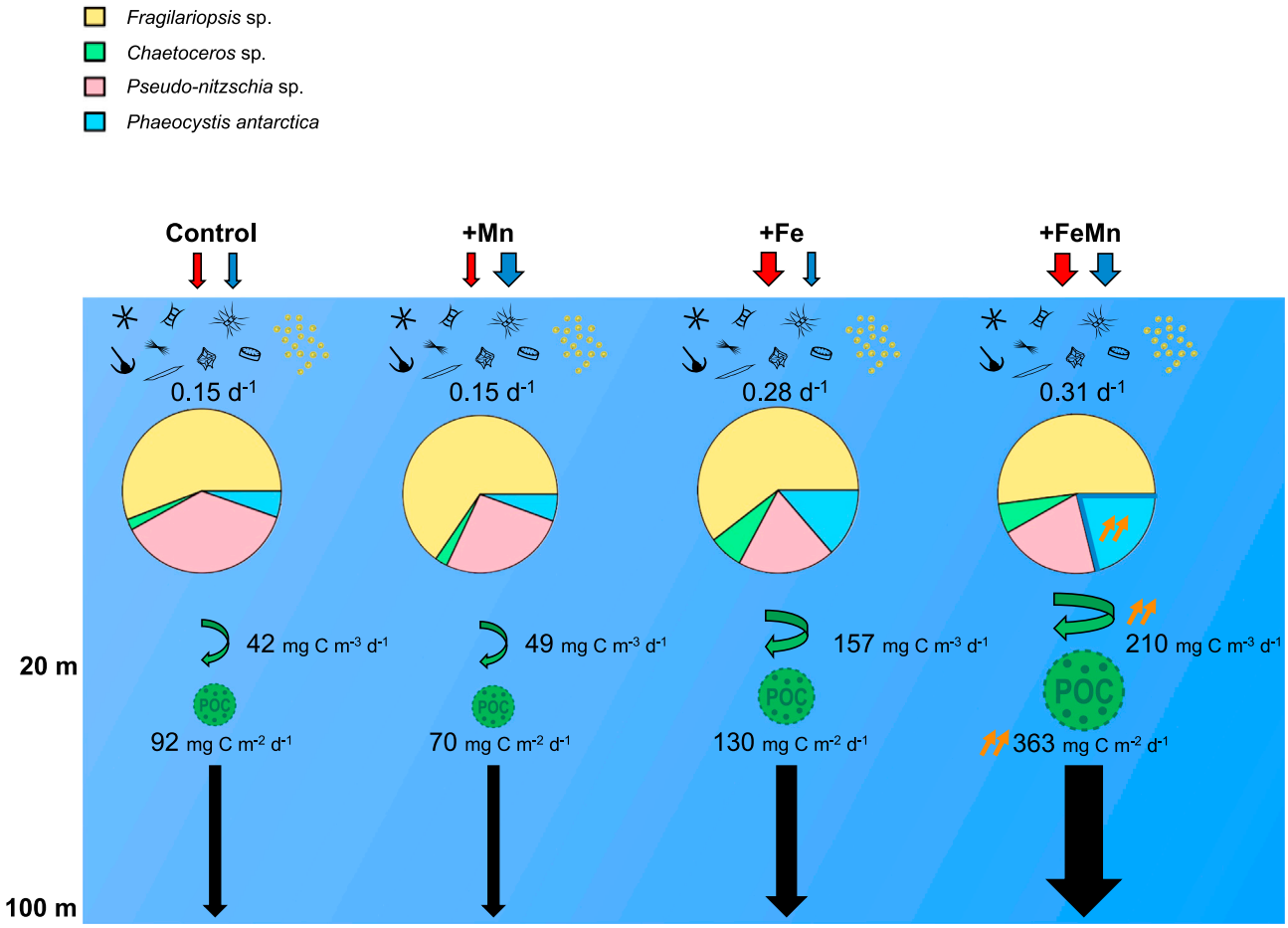

Figure 3. Effect of Fe and Mn addition on the export of organic carbon

The enhancement of the Chla-based growth rate of the whole community was mainly driven by Fe additions (+Fe: 0.28 day^{-1}, +FeMn: 0.31 day^{-1}). The additions of Fe and FeMn changed the community structure and led to an increased growth rate of *P. antarctica* (represented in blue in the pie charts), but the most significant increase (indicated by the orange arrows) resulted from FeMn addition. As a consequence, Fe and FeMn additions also increased primary production rates of the whole community (green arrows) up to 157 and 210 mg C m^{-3} day^{-1}, respectively. Still, the most significant increases (indicated by the orange arrows) resulted from FeMn addition. The higher contribution of *P. antarctica* in the FeMn treatment enhanced highly POC-enriched aggregates (green circles). The estimated carbon flux to 100 m (POC_{100_exp}, Table S3, dark arrow) was significantly influenced by the addition of Fe (130 mg C m^{-2} day^{-1}). Only the addition of FeMn increased the POC_{100_exp} up to 363 mg C m^{-2} day^{-1}, significantly higher relative to the single addition of Fe (+180%, indicated by the orange arrows).

- QUANTIFICATION AND STATISTICAL ANALYSIS

SUPPLEMENTAL INFORMATION

Supplemental information can be found online at https://doi.org/10.1016/j.cub.2023.08.086.

ACKNOWLEDGMENTS

J.B. was funded by the Deutsche Forschungsgemeinschaft (DFG) in the framework of the priority programme's Antarctic Research with comparative investigations in Arctic ice areas' project TR 899/4-1. F.K. was supported by the INSPIRE Program of the Alfred Wegener Institute. C.M.F. was supported by

Table 4. POC content of phytoplankton aggregates

	POC_{start} (mg C L^{-1})	POC_{end} (mg C L^{-1})	POC_{100_exp} (mg C m^{-2} day^{-1})
Control	0.33 ± 0.00b	5.12 ± 1.05b	92.16 ± 18.90
+Mn	0.30 ± 0.01b	6.89 ± 2.34b	70.38 ± 23.87
+Fe	0.47 ± 0.01a	7.62 ± 1.30b	129.87 ± 22.23
+FeMn	0.52 ± 0.03a	12.76 ± 3.25a	362.70 ± 92.53

Particulate organic carbon content before (POC_{start}) and after (POC_{end}) being incubated in the roller tank and POC flux to 100 m (POC_{100_exp}) were estimated from the community sampled at the end of the roller tank experiment. Values represent the mean ± SD (n = 3). Different letters indicate significant differences at the 5% level from the higher mean (a) to the lowest mean (c). For more information on POC_{100_exp}, please see Table S3.

the AWI Strategy Fund project EcoPump, and M.H.I. was supported by the Deutsche Forschungsgemeinschaft Research Center of Excellence "The Ocean Floor – Earth's Uncharted Interface" (grant EXC-2077-390741603), the framework of the Helmholtz-Gemeinschaft Deutscher Forschungszentren infrastructure program FRAM (Frontiers in Arctic Marine Monitoring) of the Alfred Wegener Institute, Helmholtz Center for Polar and Marine Research. We also would like to thank Barbara Glemser and Henning Hellmer for the support in the laboratory. Finally, we would like to thank Dr. Hartmuth Hellmer and the captain and crew of RV Polarstern during PS124.

AUTHOR CONTRIBUTIONS

J.B., S.T., and F.K. designed the experiment. J.B., F.K., and C.V. conducted the bottle experiment, measured the samples, and analyzed the data. J.B. and C.M.F. conducted the aggregation experiment; and J.B., C.M.F., and M.H.I. analyzed the data. J.B. wrote the manuscript with critical feedback from S.T., F.K., C.M.F., and M.H.I.

DECLARATION OF INTERESTS

The authors declare no competing interests.

INCLUSION AND DIVERSITY

We support inclusive, diverse, and equitable conduct of research.

Received: January 30, 2023
Revised: July 17, 2023
Accepted: August 30, 2023
Published: September 27, 2023

REFERENCES

1. Volk, T., and Hoffert, M.I. (1985). Ocean carbon pumps: analysis of relative strengths and efficiencies in ocean-driven atmospheric CO_2 changes. In The Carbon Cycle and Atmospheric CO_2: Natural Variations Archean to Present, *32* (Wiley), pp. 99–110.
2. Marinov, I., Gnanadesikan, A., Toggweiler, J.R., and Sarmiento, J.L. (2006). The Southern Ocean biogeochemical divide. Nature *441*, 964–967.
3. Deacon, G.E.R. (1979). The Weddell gyre. Deep Sea Res. Part I Oceanogr. Res. Pap. *26*, 981–995.
4. Arrigo, K.R., van Dijken, G.L., and Bushinsky, S. (2008). Primary production in the Southern Ocean, 1997–2006. J. Geophys. Res. *113*.
5. Martin, J.H., Fitzwater, S.E., and Gordon, R.M. (1990). Iron deficiency limits phytoplankton growth in Antarctic waters. Global Biogeochem. Cycles *4*, 5–12.
6. Buma, A.G.J., De Baar, H.J.W., Nolting, R.F., and Van Bennekom, A.J. (1991). Metal enrichment experiments in the Weddell-Scotia Seas: effects of iron and manganese on various plankton communities. Limnol. Oceanogr. *36*, 1865–1878.
7. Browning, T.J., Bouman, H.A., Henderson, G.M., Mather, T.A., Pyle, D.M., Schlosser, C., Woodward, E.M.S., and Moore, C.M. (2014). Strong responses of Southern Ocean phytoplankton communities to volcanic ash. Geophys. Res. Lett. *41*, 2851–2857.
8. Browning, T.J., Achterberg, E.P., Engel, A., and Mawji, E. (2021). Manganese co-limitation of phytoplankton growth and major nutrient drawdown in the Southern Ocean. Nat. Commun. *12*, 884.
9. Pausch, F., Bischof, K., and Trimborn, S. (2019). Iron and manganese co-limit growth of the Southern Ocean diatom Chaetoceros debilis. PLoS One *14*, e0221959.
10. Wu, M., McCain, J.S.P., Rowland, E., Middag, R., Sandgren, M., Allen, A.E., and Bertrand, E.M. (2019). Manganese and iron deficiency in Southern Ocean Phaeocystis antarctica populations revealed through taxon-specific protein indicators. Nat. Commun. *10*, 3582.
11. Balaguer, J., Koch, F., Hassler, C., and Trimborn, S. (2022). Iron and manganese co-limit the growth of two phytoplankton groups dominant at two locations of the Drake Passage. Commun. Biol. *5*, 207.
12. Martin, J.H., Gordon, R.M., and Fitzwater, S.E. (1990). Iron in Antarctic waters. Nature *345*, 156–158.
13. Middag, R., de Baar, H.J.W., Laan, P., Cai, P.H., and van Ooijen, J.C. (2011). Dissolved manganese in the Atlantic sector of the Southern Ocean. Deep Sea Res. Part II Top. Stud. Oceanogr. *58*, 2661–2677.
14. Twining, B.S., and Baines, S.B. (2013). The trace metal composition of marine phytoplankton. Ann. Rev. Mar. Sci. *5*, 191–215.
15. Behrenfeld, M.J., and Milligan, A.J. (2013). Photophysiological expressions of iron stress in phytoplankton. Ann. Rev. Mar. Sci. *5*, 217–246.
16. Raven, J.A., Evans, M.C.W., and Korb, R.E. (1999). The role of trace metals in photosynthetic electron transport in O2-evolving organisms. Photosynth. Res. *60*, 111–150.
17. Raven, J.A. (1990). Predictions of Mn and Fe use efficiencies of phototrophic growth as a function of light availability for growth and of C assimilation pathway. New Phytol. *116*, 1–18.
18. Hawco, N.J., Tagliabue, A., and Twining, B.S. (2022). Manganese limitation of phytoplankton physiology and productivity in the Southern Ocean. Global Biogeochem. Cycles *36*. e2022GB007382.
19. Anugerahanti, P., and Tagliabue, A. (2023). Process controlling iron–manganese regulation of the Southern Ocean biological carbon pump. Philos. Trans. A Math. Phys. Eng. Sci. *381*, 20220065.
20. Arrigo, K.R. (2005). Marine microorganisms and global nutrient cycles. Nature *437*, 349–355.
21. Riebesell, U., and Wolf-Gladrow, D.A. (1992). The relationship between physical aggregation of phytoplankton and particle flux: a numerical model. Deep Sea Res. Part I Oceanogr. Res. Pap. *39*, 1085–1102.
22. Tréguer, P., Bowler, C., Moriceau, B., Dutkiewicz, S., Gehlen, M., Aumont, O., Bittner, L., Dugdale, R., Finkel, Z., Iudicone, D., et al. (2018). Influence of diatom diversity on the ocean biological carbon pump. Nat. Geosci. *11*, 27–37.
23. Assmy, P., Smetacek, V., Montresor, M., Klaas, C., Henjes, J., Strass, V.H., Arrieta, J.M., Bathmann, U., Berg, G.M., Breitbarth, E., et al. (2013). Thick-shelled, grazer-protected diatoms decouple ocean carbon and silicon cycles in the iron-limited Antarctic Circumpolar Current. Proc. Natl. Acad. Sci. USA *110*, 20633–20638.
24. Passow, U., and Alldredge, A.L. (1995). Aggregation of a diatom bloom in a mesocosm: the role of transparent exopolymer particles (TEP). Deep Sea Res. Part II Top. Stud. Oceanogr. *42*, 99–109.
25. Passow, U. (2002). Transparent exopolymer particles (TEP) in aquatic environments. Prog. Oceanogr. *55*, 287–333.
26. Engel, A. (2000). The role of transparent exopolymer particles (TEP) in the increase in apparent particle stickiness (α) during the decline of a diatom bloom. J. Plankton Res. *22*, 485–497.
27. Mari, X., Passow, U., Migon, C., Burd, A.B., and Legendre, L. (2017). Transparent exopolymer particles: effects on carbon cycling in the ocean. Prog. Oceanogr. *151*, 13–37.
28. Asper, V.L., Deuser, W.G., Knauer, G.A., and Lohrenz, S.E. (1992). Rapid coupling of sinking particle fluxes between surface and deep ocean waters. Nature *357*, 670–672.
29. Pollard, R.T., Salter, I., Sanders, R.J., Lucas, M.I., Moore, C.M., Mills, R.A., Statham, P.J., Allen, J.T., Baker, A.R., Bakker, D.C., et al. (2009). Southern Ocean deep-water carbon export enhanced by natural iron fertilization. Nature *457*, 577–580.
30. Blain, S., Quéguiner, B., Armand, L., Belviso, S., Bombled, B., Bopp, L., Bowie, A., Brunet, C., Brussaard, C., Carlotti, F., et al. (2007). Effect of natural iron fertilization on carbon sequestration in the Southern Ocean. Nature *446*, 1070–1074.
31. Hopkinson, B.M., Mitchell, B.G., Reynolds, R.A., Wang, H., Selph, K.E., Measures, C.I., Hewes, C.D., Holm-Hansen, O., and Barbeau, K.A. (2007). Iron limitation across chlorophyll gradients in the southern Drake

Passage: phytoplankton responses to iron addition and photosynthetic indicators of iron stress. Limnol. Oceanogr. *52*, 2540–2554.

32. Behrenfeld, M.J., and Kolber, Z.S. (1999). Widespread iron limitation of phytoplankton in the South Pacific Ocean. Science *283*, 840–843.
33. Rijkenberg, M.J., Middag, R., Laan, P., Gerringa, L.J., van Aken, H.M., Schoemann, V., de Jong, J.T., and De Baar, H.J. (2014). The distribution of dissolved iron in the West Atlantic Ocean. PLoS One *9*, e101323.
34. Middag, R., De Baar, H.J.W., Laan, P., and Huhn, O. (2012). The effects of continental margins and water mass circulation on the distribution of dissolved aluminum and manganese in Drake Passage. J. Geophys. Res. *117*.
35. Middag, R., de Baar, H.J.W., Klunder, M.B., and Laan, P. (2013). Fluxes of dissolved aluminum and manganese to the Weddell Sea and indications for manganese co-limitation. Limnol. Oceanogr. *58*, 287–300.
36. Gervais, F., Riebesell, U., and Gorbunov, M.Y. (2002). Changes in primary productivity and chlorophyll a in response to iron fertilization in the Southern Polar Frontal Zone. Limnol. Oceanogr. *47*, 1324–1335.
37. Hoffmann, L.J., Peeken, I., and Lochte, K. (2007). Effects of iron on the elemental stoichiometry during EIFEX and in the diatoms *Fragilariopsis kerguelensis* and *Chaetoceros dichaeta*. Biogeosciences *4*, 569–579.
38. Arrigo, K.R., Robinson, D.H., Worthen, D.L., Dunbar, R.B., DiTullio, G.R., VanWoert, M., and Lizotte, M.P. (1999). Phytoplankton community structure and the drawdown of nutrients and CO_2 in the Southern Ocean. Science *283*, 365–367.
39. Schoemann, V., Becquevort, S., Stefels, J., Rousseau, V., and Lancelot, C. (2005). Phaeocystis blooms in the global ocean and their controlling mechanisms: a review. J. Sea Res. *53*, 43–66.
40. Nöthig, E.-M., Assmy, P., Klaas, C., and Scharek, R. (2009). Phyto-and protozooplankton in polar waters. In Biological Studies in Polar Oceans: Exploration of Life in Icy Waters; 35 Research Reports and Reviews, G. Hempel, and I. Hempel, eds. (Wirtschaftsverl. NW, Verl. für neue Wissenschaft), pp. 65–73.
41. Boyd, P.W., Jickells, T., Law, C.S., Blain, S., Boyle, E.A., Buesseler, K.O., Coale, K.H., Cullen, J.J., De Baar, H.J., and Follows, M. (2007). Mesoscale iron enrichment experiments 1993–2005: synthesis and future directions. Science *315*, 612–617.
42. de Baar, H.J.W., Boyd, P.W., Coale, K.H., Landry, M.R., Tsuda, A., Assmy, P., Bakker, D.C., Bozec, Y., Barber, R.T., and Brzezinski, M.A. (2005). Synthesis of iron fertilization experiments: from the Iron Age in the Age of Enlightenment. J. Geophys. Res. *110*.
43. Smetacek, V., and Naqvi, S.W.A. (2008). The next generation of iron fertilization experiments in the Southern Ocean. Philos. Trans. A Math. Phys. Eng. Sci. *366*, 3947–3967.
44. Geider, R.J., and La Roche, J. (1994). The role of iron in phytoplankton photosynthesis, and the potential for iron-limitation of primary productivity in the sea. Photosynth. Res. *39*, 275–301.
45. van Leeuwe, M.A., and Stefels, J. (1998). Effects of iron and light stress on the biochemical composition of Antarctic *Phaeocystis* sp. (Prymnesiophyceae). II. Pigment composition. J. Phycol. *34*, 496–503.
46. Hoffmann, L.J., Peeken, I., Lochte, K., Assmy, P., and Veldhuis, M. (2006). Different reactions of Southern Ocean phytoplankton size classes to iron fertilization. Limnol. Oceanogr. *51*, 1217–1229.
47. Peers, G., and Price, N.M. (2004). A role for manganese in superoxide dismutases and growth of iron-deficient diatoms. Limnol. Oceanogr. *49*, 1774–1783.
48. Gall, M.P., Boyd, P.W., Hall, J., Safi, K.A., and Chang, H. (2001). Phytoplankton processes. Part 1: community structure during the Southern Ocean iron release experiment (SOIREE). Deep Sea Res. Part II Top. Stud. Oceanogr. *48*, 2551–2570.
49. Marchetti, A., Maldonado, M.T., Lane, E.S., and Harrison, P.J. (2006). Iron requirements of the pennate diatom Pseudo-nitzschia: comparison of oceanic (high-nitrate, low-chlorophyll waters) and coastal species. Limnol. Oceanogr. *51*, 2092–2101.
50. Bertrand, E.M., Saito, M.A., Rose, J.M., Riesselman, C.R., Lohan, M.C., Noble, A.E., Lee, P.A., and DiTullio, G.R. (2007). Vitamin B12 and iron colimitation of phytoplankton growth in the Ross Sea. Limnol. Oceanogr. *52*, 1079–1093.
51. Koch, F., and Trimborn, S. (2019). Limitation by Fe, Zn, Co, and B12 results in similar physiological responses in two Antarctic phytoplankton species. Front. Mar. Sci. *6*, 514.
52. Calvo-Díaz, A., Díaz-Pérez, L., Suárez, L.Á., Morán, X.A.G., Teira, E., and Marañón, E. (2011). Decrease in the autotrophic-to-heterotrophic biomass ratio of picoplankton in oligotrophic marine waters due to bottle enclosure. Appl. Environ. Microbiol. *77*, 5739–5746.
53. Venrick, E.L., Beers, J.R., and Heinbokel, J.F. (1977). Possible consequences of containing microplankton for physiological rate measurements. J. Exp. Mar. Biol. Ecol. *26*, 55–76.
54. Bender, S.J., Moran, D.M., McIlvin, M.R., Zheng, H., McCrow, J.P., Badger, J., DiTullio, G.R., Allen, A.E., and Saito, M.A. (2018). Colony formation in *Phaeocystis antarctica*: connecting molecular mechanisms with iron biogeochemistry. Biogeosciences *15*, 4923–4942.
55. Balaguer, J., Thoms, S., and Trimborn, S. (2023). The physiological response of an Antarctic key phytoplankton species to low iron and manganese concentrations.. Published online August 1, 2023. Limnol. Oceanogr..
56. Schoemann, V., Wollast, R., Chou, L., and Lancelot, C. (2001). Effects of photosynthesis on the accumulation of Mn and Fe by Phaeocystis colonies. Limnol. Oceanogr. *46*, 1065–1076.
57. Hassler, C.S., and Schoemann, V. (2009). Bioavailability of organically bound Fe to model phytoplankton of the Southern Ocean. Biogeosciences *6*, 2281–2296.
58. Hassler, C.S., Schoemann, V., Nichols, C.M., Butler, E.C., and Boyd, P.W. (2011). Saccharides enhance iron bioavailability to Southern Ocean phytoplankton. Proc. Natl. Acad. Sci. USA *108*, 1076–1081.
59. Hamm, C.E., Simson, D.A., Merkel, R., and Smetacek, V. (1999). Colonies of Phaeocystis globosa are protected by a thin but tough skin. Mar. Ecol. Prog. Ser. *187*, 101–111.
60. Matrai, P.A., Vernet, M., Hood, R., Jennings, A., Brody, E., and Saemundsdottir, S. (1995). Light-dependence of carbon and sulfur production by polar clones of the genus Phaeocystis. Mar. Biol. *124*, 157–167.
61. Mathot, S., Smith, W.O., Jr., Carlson, C.A., Garrison, D.L., Gowing, M.M., and Vickers, C.L. (2000). Carbon partitioning within Phaeocystis antarctica (Prymnesiophyceae) colonies in the Ross Sea, Antarctica. J. Phycol. *36*, 1049–1056.
62. Morris, P.J., Sanders, R., Turnewitsch, R., and Thomalla, S. (2007). 234th-derived particulate organic carbon export from an island-induced phytoplankton bloom in the Southern Ocean. Deep Sea Res. Part II Top. Stud. Oceanogr. *54*, 2208–2232.
63. Measures, C.I., Brown, M.T., Selph, K.E., Apprill, A., Zhou, M., Hatta, M., and Hiscock, W.T. (2013). The influence of shelf processes in delivering dissolved iron to the HNLC waters of the Drake Passage, Antarctica. Deep Sea Res. Part II Top. Stud. Oceanogr. *90*, 77–88.
64. Wang, S., and Moore, J.K. (2011). Incorporating Phaeocystis into a Southern Ocean ecosystem model. J. Geophys. Res. Oceans *116*.
65. Nissen, C., and Vogt, M. (2021). Factors controlling the competition between *Phaeocystis* and diatoms in the Southern Ocean and implications for carbon export fluxes. Biogeosciences *18*, 251–283.
66. Latour, P., Wuttig, K., van der Merwe, P., Strzepek, R.F., Gault-Ringold, M., Townsend, A.T., Holmes, T.M., Corkill, M., and Bowie, A.R. (2021). Manganese biogeochemistry in the Southern Ocean, from Tasmania to Antarctica. Limnol. Oceanogr. *66*, 2547–2562.
67. Schlitzer, R. (2015). Ocean data view. https://odv.awi.de/.
68. Cutter, G.A., Casciotti, K., Croot, P., Geibert, W., Heimbürger, L.-E., Lohan, M.C., Planquette, H., and van de Flierdt, T. (2017). Sampling and sample-handling protocols for GEOTRACES cruises. Version 3.0 (Ocean Best Practices).

69. Gerringa, L.J.A., De Baar, H.J.W., and Timmermans, K.R. (2000). A comparison of iron limitation of phytoplankton in natural oceanic waters and laboratory media conditioned with EDTA. Mar. Chem. *68*, 335–346.

70. Schindelin, J., Arganda-Carreras, I., Frise, E., Kaynig, V., Longair, M., Pietzsch, T., Preibisch, S., Rueden, C., Saalfeld, S., Schmid, B., et al. (2012). Fiji: an open-source platform for biological-image analysis. Nat. Methods *9*, 676–682.

71. Meijering, E., Dzyubachyk, O., and Smal, I. (2012). Methods for cell and particle tracking. Methods Enzymol. *504*, 183–200.

72. Ploug, H., Terbrüggen, A., Kaufmann, A., Wolf-Gladrow, D., and Passow, U. (2010). A novel method to measure particle sinking velocity in vitro, and its comparison to three other in vitro methods. Limnol. Oceanogr.: Methods *8*, 386–393.

73. Martin, J.H., Knauer, G.A., Karl, D.M., and Broenkow, W.W. (1987). VERTEX: carbon cycling in the northeast Pacific. Deep Sea Res. Part I Oceanogr. Res. Pap. *34*, 267–285.

74. Buesseler, K.O., Boyd, P.W., Black, E.E., and Siegel, D.A. (2020). Metrics that matter for assessing the ocean biological carbon pump. Proc. Natl. Acad. Sci. USA *117*, 9679–9687.

75. Hathorne, E.C., Haley, B., Stichel, T., Grasse, P., Zieringer, M., and Frank, M. (2012). Online preconcentration ICP-MS analysis of rare earth elements in seawater. Geochem. Geophys. Geosyst. *13* (1).

76. Rapp, I., Schlosser, C., Rusiecka, D., Gledhill, M., and Achterberg, E.P. (2017). Automated preconcentration of Fe, Zn, Cu, Ni, Cd, Pb, Co, and Mn in seawater with analysis using high-resolution sector field inductively-coupled plasma mass spectrometry. Anal. Chim. Acta *976*, 1–13.

77. Biller, D.V., and Bruland, K.W. (2012). Analysis of Mn, Fe, Co, Ni, Cu, Zn, Cd, and Pb in seawater using the Nobias-chelate PA1 resin and magnetic sector inductively coupled plasma mass spectrometry (ICP-MS). Mar. Chem. *130–131*, 12–20.

78. Moore, C.M., Mills, M.M., Arrigo, K.R., Berman-Frank, I., Bopp, L., Boyd, P.W., Galbraith, E.D., Geider, R.J., Guieu, C., Jaccard, S.L., et al. (2013). Processes and patterns of oceanic nutrient limitation. Nat. Geosci. *6*, 701–710.

79. Utermöhl, H. (1958). Zur vervollkommnung der quantitativen phytoplankton-methodik: Mit 1 Tabelle und 15 abbildungen im Text und auf 1 Tafel. SIL Communications, 1953-1996: Internationale Vereinigung für theoretische und angewandte Limnologie *9*, 1–38.

80. Tomas, C.R., and Haste, G.R. (1997). Identifying Marine Phytoplankton (Academic Press).

81. Mathot, S., Smith, W.O., Jr., Carlson, C.A., and Garrison, D.L. (2000). Estimate of Phaeocystis sp. carbon biomass: methodological problems related to the mucilaginous nature of the colonial matrix. J. Phycol. *36*, 1049–1056.

82. Olson, R.J., Zettler, E.R., Chisholm, S.W., and Dusenberry, J.A. (1991). Advances in oceanography through flow cytometry. In Part. Anal. Oceanogr. (Springer), pp. 351–399.

83. Welschmeyer, N.A. (1994). Fluorometric analysis of chlorophyll a in the presence of chlorophyll b and pheopigments. Limnol. Oceanogr. *39*, 1985–1992.

84. Intergovernmental Oceanographic Commission (1994). Protocols for the Joint Global Ocean Flux Study (JGOFS) core measurement (UNESCO), pp. 97–100.

85. Oxborough, K., Moore, C.M., Suggett, D.J., Lawson, T., Chan, H.G., and Geider, R.J. (2012). Direct estimation of functional PSII reaction center concentration and PSII electron flux on a volume basis: a new approach to the analysis of fast repetition rate fluorometry (FRRf) data. Limnol. Oceanogr.: Methods *10*, 142–154.

86. Stoll, M.H.C., Bakker, K., Nobbe, G.H., and Haese, R.R. (2001). Continuous-flow analysis of dissolved inorganic carbon content in seawater. Anal. Chem. *73*, 4111–4116.

STAR★METHODS

KEY RESOURCES TABLE

REAGENT or RESOURCE	SOURCE	IDENTIFIER
Biological samples		
Phytoplankton natural communities	This paper	https://doi.org/10.1594/PANGAEA.957278
Deposited data		
Original dataset	PANGAEA	https://doi.org/10.1594/PANGAEA.957278
Software and algorithms		
R Studio version 1.1.463, © 2009-2016 R library – 'stats'	R Core Team and contributors worldwide	https://www.r-project.org/
R Studio version 1.1.463, © 2009-2016 R library – 'agricolae'	Felipe de Mendiburu	https://cran.r-project.org/web/packages/agricolae/agricolae.pdf
Ocean Data View	Schlitzer[67]	N/A

RESOURCE AVAILABILITY

Lead contact

Further information and requests for resources should be directed to and will be fulfilled by the Lead Contact, Jenna Balaguer.

Materials and data availability

All data needed to evaluate the conclusions in the paper are present in the manuscript and/or Supplementary Materials and will be freely available from the PANGAEA data repository.

Data and code availability

· Microscopy data reported in this study will be shared by the lead contact upon request.
· This study does not report any original code.
· Any additional information required to reanalyze the data reported in this paper is available at https://doi.org/10.1594/PANGAEA.957278 as well from the lead contact upon request.

EXPERIMENTAL MODEL AND SUBJECT DETAILS

The study was performed *in vivo* with a natural phytoplankton community. The water for the experiment was taken during RV Polarstern COSMUS expedition PS124 (January to April 2021), the 28.02.21 at 76° 06.140 30° 19.084.

METHOD DETAILS

Water collection for *in situ* sampling and one shipboard phytoplankton TM incubation experiment

In situ sampling: During the RV Polarstern COSMUS expedition PS124 (January to April 2021), a Teflon CTD equipped with GoFlo bottles (12L/bottle capacity) was used to sample 6 *in situ* stations (Figure 1A, Stations 1-6) in the southern Weddell Sea to determine concentrations of total dissolved iron (dFe) and dissolved manganese (dMn) to derive the dMn deficiency rate relative to dFe (Mn*)[8] in surface water (20 m depth). TM clean techniques, based on GEOTRACES guidelines[68] were used in all sampling and sample processing. To minimize potential TM contamination, the GoFlo bottles were sampled directly in a clean laboratory container under a laminar flow bench (US class 100, Opta, Bensheim, Germany). All tubing, carboys, bottles, and other equipment used for TM sampling were sequentially soaked for 1 week in 1% Citranox and for 1 week in 1.2 mol L^{-1} hydrochloric acid (PA grade, Merck Millipore Corporation, Darmstadt, Germany). Between each soaking step, the bottles were rinsed 7 times with ultrapure water (Merck Millipore Corporation, Darmstadt, Germany). Finally, the equipment/bottles were air-dried under a clean bench (US class 100, Opta, Bensheim, Germany) and packed in two polyethylene bags for storage. For the 6 stations, primary production rates were also quantified. Please note that the detailed method description for the TM analysis and primary production measurements will be given below.

In addition, the particulate organic carbon flux down to 100 m depth (POC_{100_insitu}) was measured from 3 sediments traps (1, 2 and 3; Table 1) in the same area (Figure 1A). The drifting sediment trap (KC Denmark) consisted of a trap station at 100m depths equipped with 4 collection cylinders attached *via* a gyroscopic mounting. The final deployment times of the 3 sediment traps varied between 18h and 26h (Table 1). Material from one trap tube per depth was fixed with 0.14% mercuric chloride and stored at 4°C for

later determination of mass and element fluxes. In the home laboratory, a sample splitter (McLane) was used to split each sample into five equal parts and particulate organic carbon (POC) was determined.

Shipboard incubation experiment: At location 1 (Figure 1A), a shipboard incubation experiment, which took place between the 28.02.21 and the 7.03.21, was conducted in order to study the effects of Fe and Mn limitations on SO phytoplankton productivity and how this impacts community structure and aggregate formation in the southern Weddell Sea. At this location, HNLC seawater was collected from a depth of 20m using TM clean techniques based on GEOTRACES guidelines.[68] To minimize potential TM contamination, seawater was pumped directly into a clean laboratory container using a Teflon membrane pump (Almatec, Futur 50). The whole system (pump and hosing) was flushed for >1 h before filling 4L polycarbonate bottles for the experiments. All tubing, carboys, incubation bottles, and other equipment used during the experiment were TM clean. The Control treatment consisted of seawater without any TM addition, while the other 3 treatments were enriched with either iron chloride ($FeCl_3$) alone (0.5 nmol L^{-1}, AAS standard, TraceCERT, Fluka; +Fe treatment), manganese chloride ($MnCl_2$) alone (1 nmol L^{-1}, AAS standard, Trace- CERT, Fluka; +Mn treatment), or together (+FeMn treatment). Low dFe and dMn concentrations for the addition treatments were chosen to reduce the formation of inorganic colloids in our experiments. No ethylenediaminetetraacetic acid (EDTA) was added to avoid alteration of the natural seawater trace metal chemistry.[69] All incubation bottles were maintained at 100 μmol photons m^{-2} s^{-1} white light under a 20:4 (light:dark) hour cycle, mimicking natural conditions typical for the time and region. The experiment was performed in a clean laboratory container set at 1°C. All treatments consisted of triplicate 4L bottles, gently rotated daily to avoid cell sedimentation. To monitor the experiment, every 2-4 days, the photosynthetic efficiency was assessed using a Fast Repetition Rate Fluorometer (FRRf, FastOcean PTX sensor, Chelsea Technologies Group (Figure S1A) and chlorophyll a, a proxy of algal biomass, was measured (Figure S1B) using a Trilogy Fluorometer (Turner Design, San Jose, CA, USA). At the start and the end of the experiment, samples were taken for the determination of seawater chemistry (Fe, Mn and macronutrients), phytoplankton productivity, community composition, elemental composition (Particulate organic carbon/nitrogen and pigments) and photophysiology. The duration of the experiment was 8 days.

To test aggregation capacity and carbon export potential of the final communities established in each treatment (Control, +Mn, +Fe, and +FeMn; Figure S2), 911 ml aliquots were taken from each triplicate bottle at the end of the incubation experiment and combined in a roller tank (d= 20 cm, L=8.7 cm, V=2733 cm^3) to induce aggregation *via* differential settling. The tanks were rotated at 1 rotation per minute (rpm) over 48h at a constant temperature of 1°C and 100 μmol photons m^{-2} s^{-1} white light under a 20:4 h (light:dark) cycle. After 24 h and 48 h, all tanks were filmed with a Canon EOS 650 to record aggregate formation, size/volume, and sinking velocity (Table S3). The whole tank was imaged to make sure that all depths were in focus. Tracking of particles was performed using the imaging software FIJI/ImageJ, for which the methodology described in Schindelin et al.[70] was applied. The abundance (Aggregates, Table S3) and size of aggregates (equivalent circular diameter, Table S3) were calculated from the aggregate area as measured in the still images of single frames extracted from the video recordings. Each aggregate was then identified in the tank and their sizes were determined as total two-dimensional pixel area. This was performed by applying a threshold to the images so each aggregate was identified as a white object against a dark background (using ImageJ). The aggregate area has been converted to an equivalent circular diameter, i.e. the number of pixels (Table S3). Using a scale bar imaged when the videos were recorded, the number of pixels can be converted to diameter in millimetres. FIJI plug-in "MTrackJ"[71] was used to track the aggregate and tank orbits which were needed to calculate the sinking velocity following Ploug et al.[72] method. At the end of the roller tank incubation, aggregated material (POC_{end}, the sum of all aggregates) was collected for POC measurements. As the bottle replicates from the incubation were combined into a single flocculation experiment, the evaluation of the uncertainty is based on the robustness and the variability of the POC measurements that were performed in triplicates.

We estimated the potential POC flux down to 100m (POC_{100_exp}, Table S3) for each treatment in order to compare it to the *in situ* measured sediment trap flux at 100m. To do this, we upscaled the aggregate formation from the roller tank incubations to get the aggregate formation in $1m^3$ of water within the upper water column. This was done by measuring the size of each aggregate formed during the roller tank incubations (S_{AGG}, Table S3). The total POC aggregation per aggregate size-class was calculated by applying the size-specific POC content to each aggregate size (POC_{AGG}, Table S3) and summing the POC content for each size-class in each treatment. This was upscaled from the roller tank volume to a cubic meter (V_{POC_AGG}, Table S3). The flux out of the upper 20m water column (F_{20}) was calculated by multiplying the total aggregated carbon concentration per size-class per cubic meter (V_{POC_AGG}, Table S3) by the size-specific (measured) sinking velocities for each size-class (S_v, Table S3). Finally, we used the Martin Curve to estimate the potential flux to 100m[73]:

$$F_z = F_{20}\left(\frac{z}{20}\right)^{-b} \quad \text{(Equation 1)}$$

where F_z (POC_{100_AGG} in Table S3) is the sinking flux of POC to the depth z (100m), F_{20} is the potential flux out of the upper 20m of the water column (estimated using the roller tank incubations). The exponent "b" defines the average attenuation of POC flux. During the cruise, *in situ* camera profiles showed strong attenuation in the total aggregate volume between 20 and 100m, we therefore used a rather high b-value of -1.29, previously observed at the Polar Front in the Southern Ocean.[74] The whole detailed calculation as well as all the parameters are provided in Table S3.

TM seawater chemistry

100 mL of seawater was filtered through polycarbonate filters (0.2 μm pore size) using a Thermo Scientific Nalgene® (300-4100) filtration system; the filtrate was collected into a polyethylene bottle and stored triple bagged at 2°C until analysis for dTM back at the lab. Concentrations of the dFe and dMn were determined on a SeaFast system (Elemental Scientific, Omaha, NE, USA)[75,76] coupled to an inductively coupled plasma mass spectrometer (ICP-MS, Element2, Thermo Fisher Scientific, resolution of R = 2000). An iminodiacetate chelation column (part number CF-N-0200, Elemental Scientific) was used during the preconcentration step. All seawater samples were acidified to pH=1.7 with a double distilled nitric acid (HNO_3) (distilled 65% HNO_3, pro analysis, Merck) and irradiated for 1.5h using a UV power supply system (7830) and Photochemical lamp (7825) from ArcGlass to provide total dissolved concentrations of trace metals and avoid the presence of organic compounds.[77] During each UV digestion step, two blanks were taken. The ICP-MS was optimized daily to achieve oxide forming rates below 0.3%. Each seawater sample was analyzed via standard addition to minimize any matrix effects which might influence the quality of the analysis. To assess the accuracy and precision of the method, a NASS-7 (National Research Council of Canada) reference standard was analyzed in a 1:10 dilution (corresponding to environmentally representative concentrations) at the beginning, in the middle and at the end of each run (two batch runs; n = 18). The analytical blanks for Fe and Mn measurements, as well as the NASS-7 certified values, can be found in the Table S4. The dissolved macronutrient concentrations (nitrate, phosphate and silicate) were determined colorimetrically in the laboratory on a QuAAtro autoanalyzer (Seal Analyticals).[86]

The Mn deficiency rate (Mn*, nmol L^{-1}) was determined from[8] :

$$Mn^* = dMn - \frac{dFe}{R}, \quad \text{(Equation 2)}$$

where R is the assumed average of phytoplankton Fe:Mn ratio (2.67).[78]

Phytoplankton community characterization

Light microscopy

To determine the effects of the different treatments on the microplankton composition, unfiltered seawater was collected at the start and the end of both experiments for later analysis via light microscopy in the home laboratory. Briefly, samples were fixed with Lugol's solution (1% final concentration) and stored at 2°C in the dark until taxonomic analysis. All samples were allowed to settle in Utermöhl sedimentation chambers (Hydrobios, Altenholz, Germany) for at least 24 hours and were analyzed on an inverted light microscope (Axiovert 200; Zeiss), according to the method of Utermöhl[79]. Different genera were counted and identified according to taxonomic literature.[80] Each aliquot was examined until at least 400 cells had been counted (Table S1). To determine the cell abundance of *P. antarctica* colonies, the relationship between colony sizes and cell number per colony was determined (Table S2; Figure S3) according to the method of Mathot et al.[81]

Flow cytometry

Autotrophic pico- (0.2 – 2 μm) and nanoeukaryotes (> 2 μm), as well as heterotrophic bacteria (< 2 μm), were analyzed via flow cytometry. At the start and the end of the experiment, samples were preserved with 10% buffered formalin, flash-frozen in liquid nitrogen. Abundances of heterotrophic bacteria (stained with Synergy Brands Green I), phycoerythrin-containing picocyanobacteria, and photosynthetic picoeukaryotes were determined by means of a BD Accuri™ C6 Plus flow cytometer (Becton, Dickinson and Company) using fluorescence patterns and particle size from side angle light scatter.[82] Before running the samples, 2 μL beads (Spherotech - Rainbow Fluorescent Particles - 2.11 μm) were added to each treatment as a size and fluorescence reference. Then pico-/nanoeukaryotes were identified based on side scatter versus FL-3 (Figure S4) and heterotrophic bacteria on side scatter versus FL-1.

Based on cell abundances, the net growth rate per day (μ, d^{-1}) was calculated for all cells using:

$$\mu = \frac{ln\left(\frac{Nt_2}{Nt_1}\right)}{dt} \quad \text{(Equation 3)}$$

where $\mathbf{N_{t1}}$ and $\mathbf{N_{t2}}$ are the cell abundances at the start and end of each incubation experiment, while ***dt*** denotes the incubation time in days.

Phytoplankton quotas

Chlorophyll a (Chla)

Chl*a* samples were taken throughout the experiment (Figure S1B). All samples were filtered onto glass-fiber filters (GF/F, ≈0.7 μm, 25 mm, Whatman, Wisconsin, USA) and were directly stored at -20°C in the dark until further analysis. Samples were extracted in 90% acetone for 24h at 4°C in the dark and analyzed fluorometrically[83] on a Trilogy Fluorometer (Turner Design, San Jose, CA, USA) using the non-acidification module. Based on Chl*a* initial and final concentrations (Table S5), a growth rate per day (μ, d^{-1}) was calculated from Equation 3.

Particular organic carbon (POC) and nitrogen (PON) content

At the start and the end of the experiment as well as from the sediment traps, seawater was filtered onto pre-combusted glass-fiber filters (15h, 500°C, GF/F, ≈0.7 μm, 25 mm, Whatman, Wisconsin, USA) and stored at -20°C in pre-combusted glass petri dishes. Prior to analysis with a Euro Elemental Analyzer 3000 CHNS-O (HEKAtech GmbH), the filters were dried for > 12h at 60°C and

then acidified with 200 μL of 0.2N HCL to remove inorganic carbon and dried a second time. Content of POC and PON (Table S5) were corrected for blank measurements and normalized to filtered volume and cell densities to yield cellular quotas. The POC-based growth rate was derived from Equation 3.

^{14}C-based primary production

Primary production was determined in 50 mL TMC culture flasks from the 6 *in situ* stations as well as the end of the incubation experiment. To this end, 0.97 MBq of ^{14}C-bicarbonate (Perkin Elmer, specific activity 2035 MBq mmol^{-1}) was added to each flask according to the JGOFS protocol,[84] and the bottles were bagged and returned to the position of the original experiment. Incubations were terminated after 24 hours by filtering samples onto 0.2 μm pore size polycarbonate filters. At the beginning and the end of the incubation, 250 μL were removed from each vial to determine total activity (the amount of isotope added). After placing the filters into scintillation vials, 250 μL of 1.2 N hydrochloric acid was added and any remaining dissolved inorganic ^{14}C was allowed to degas for 24h. 5 mL of Ultima Gold (Perkin Elmer) was then added to each vial and the samples were analyzed on a Scintillation Counter (Tri-Carb 2900 TR, Perkin Elmer) onboard. Net primary production rates were then calculated as described in the JGOFS protocol.[84]

Photosystem II (PSII) fluorescence

At the start, during (every 2-4 days) and at the end of the experiment (Figure S1A), Chl*a* fluorescence measurements were collected using a Fast Repetition Rate Fluorometer (FRRf) coupled to a FastAct Laboratory system (FastOcean PTX), both from Chelsea Technologies Group. Chl*a* fluorescence of PSII was determined after 1 h of dark acclimation prior measurements to ensure that all photosystems' II reaction centres were oxidized.

The single turnover mode was set with a saturation phase of 100 flashlets on a 2 μs pitch in order to saturate photosystem II and followed by a relaxing phase of 40 flashlets on a 50 μs pitch. From these measurements, the minimum (F_0) and maximum (F_m) were derived to calculate the maximum quantum yield of PSII (F_v/F_m [rel. unit]):

$$\frac{F_v}{F_m} = (F_m - F_0)/F_m \quad \text{(Equation 4)}$$

From Oxborough et al.,[85] the functional absorption cross sections of PSII (σ_{PSII}, nm^2 PSII^{-1}) were derived using the FastPro8 Software (Version 1.0.55, Kevin Oxborough, CTG Ltd).

QUANTIFICATION AND STATISTICAL ANALYSIS

Shapiro-Wilk tests were performed to test the normal distribution and equal variances of the datasets. A one-way analysis of variance (ANOVA) was conducted to assess the impact of Fe and Mn availability compared to the Control treatment on cell abundance and Chl*a* accumulation rate. As post-hoc tests, the Fisher Least Significant Difference (LSD) was used between the mean group for a comparison of the effect of all factors. A $p < 0.05$ was used to establish significant differences among treatments. All statistical analyses were performed with R Studio (version 1.1.463, © 2009-2016) and all maps with Ocean Data View.[67] R packages to reproduce statistical analysis are 'stats' and 'agricolae'.